Application of nonlinear dynamics analysis to gas-solid flow system in horizontal pneumatic conveying of plastic pellets

Osamh S. Alshahed [a,*], Baldeep Kaur [a], Michael S.A. Bradley [a], David Armour-Chelu [b]

[a] Wolfson Centre for Bulk Solids Handling Technology, University of Greenwich, Kent ME4 4TB, UK
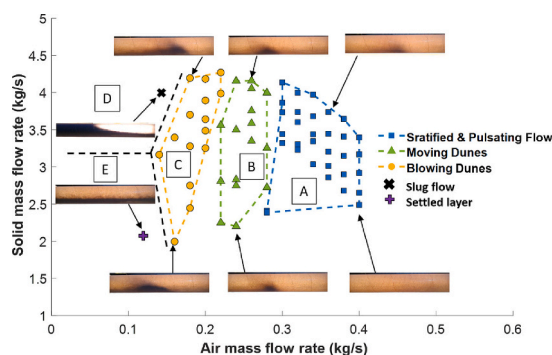[b] School of Engineering, University of Greenwich, Kent ME4 4TB, UK

HIGHLIGHTS

- Developed pneumatic conveying state diagram classified with flow patterns.
- Measured pressure and electrostatic fluctuations of horizontal gas-solid flows.
- Recurrence plots of classified flow patterns showed different structures.
- Proposed correlations between nonlinear dynamics measures and state diagram.
- Nonlinear dynamics measures revealed minimum energy consumption operations.

GRAPHICAL ABSTRACT

Flow pattern map developed for horizontal pneumatic conveying of plastic pellets.

ABSTRACT

Chaotic invariant and recurrence quantification analysis measures have characterised fully developed gas-solid flow in horizontal pneumatic conveying of plastic pellets. These measures describe the complexity in phase spaces (attractors) and recurrence plots, reconstructed from pressure and bottom arc-shaped electrostatic signals to characterise the behaviour of flow patterns. Different flow patterns were identified using high-speed video imaging of a transparent pipeline and classified at several operating conditions in a flow pattern map and state diagram. Recurrence plots were analysed for the identified flow patterns, which showed different qualitative structures. The chaotic invariant and recurrence quantification analysis measures were correlated with the state diagram, indicating that the fluctuations of pressure senor and electrostatic sensor signals can classify the flow patterns at different operating conditions. Combining the analysis measures for electrostatic signals can indicate whether the flow condition is above, near or below the minimum energy consumption operating conditions.

1. Introduction

The pneumatic conveying system has three primary modes of

operation: dilute phase, transition phase and dense phase. Choosing between these phases during conveying can be challenging depending on the material properties, conveying route structure and distance, and pressure availability in the pipelines. Dilute phase flow operation is

---

* Corresponding author.
E-mail address: osamhsabrialshahed@gmail.com (O.S. Alshahed).

List of symbols

MCAV	Minimum conveying air velocity, m/s
PMC	Pressure drop minimum curve, Pa/m
m_s	Solids mass flow rate, kg/s
m_a	Air mass flow rate, kg/s
P1 to P8	Pressure sensor tapings
t	Time, s
x(t)	Data point value at specific, t
τ	Time delay
m	Embedding dimension
n	Number of data points
N	Number of phase points
$Y(t)$	Phase space (Time series vector)
FNN	False nearest neighbour algorithm
i and j	Subscript for phase points indexes
r	Radius of a hypersphere
$Cr(r)$	Correlation integral function
$\Theta(h)$	Heaviside step function
r_{Cr1}, r_{Cr2}	Radius hypersphere limits for correlation integral scalling region
CD	Correlation dimension
s	Subscript for nearest neighbour phase point index
k	Subscript for Expansion step index
k_{Min}	Minimum expansion step
k_{Max}	Maximum expansion step
dt	Time difference between acquired data points
$\lambda(i)$	Lyapunov exponent
$ALDiv$	Average log divergence
LE	Largest Lyapunov exponent
Φ	Statistical function
AE	Approximate entropy
AE_{max}	Maximum approximate entropy across different radius hypersphere
r_{AEmax}	Radius hypersphere at maximum approximate entropy
RP	Recurrence plot Matrix
r_{RP}	Radius hypersphere threshold for recurrence plot development
LOI	Line of Identity in a recurrence plot
LWA	Local white areas
LBA	Local bolt areas
RQA	Recurrence quantification analysis
RR	Recurrence rate
DET	Recurrence plot determinism
E	Recurrence plot entropy
l	Diagonal line length
l_{min}	Minimum diagonal line length
$P(l)$	Histogram of diagonal lines
L	Average diagonal line length

generally considered when a simple pneumatic conveying system design is required to achieve a stable and reliable operation [1]. Dilute phase flow operates at a high gas velocity in large volumes and low solid concentrations of particles, where discrete particles are uniformly suspended via drag and lift forces caused by turbulent air stream [2]. In practice, pneumatically conveying solids at high gas velocity often result in high energy consumption, material degradation and pipeline wear [3]. Dense phase flow operation is characterised by a high concentration of particles and low gas velocity, resulting in improved product quality and reduced pipeline sizing and wear rate [4]. However, the dense phase flow operation requires more pressure availability resulting in a high initial cost of equipment to withstand high-pressure operations.

The flow pattern map and the state diagram describe the gas-solid flow transition spectrum from dilute to dense phase flow operations for specific particulate material. The flow pattern map shows a distribution of operating condition points, including air mass flow rate (m_a) and solids mass flow rate (m_s), classified according to the observed flow patterns in a transparent pipeline [5,6]. The state diagram is a function that relates average air velocity with air pressure drop per unit length of a pipeline having a constant inner diameter [5,7]. The pressure drop directly relates to the air velocity in dilute phase flow operation and shifts to an indirect relationship for dense phase flow. The air velocity at the centre of this shifting curve is the optimal conveying condition, known as minimum conveying air velocity (MCAV). While the pressure drop line connecting the MCAV at different solids mass flow rates is known as the pressure drop minimum curve (PMC). The instabilities of flow patterns in the transition phase from dilute to dense phase flow increase as the operating conditions approach the PMC. Operating the pneumatic conveying system at or below the MCAV may lead to a sudden blockage in the pipeline depending on the air velocity, solids mass flow rate and material properties.

Operating at a gas velocity close to the MCAV in a horizontal pipeline leads to particle accumulations at the bottom of the pipeline cross-section with a nonuniform distribution. These accumulations form dense clusters with a high solid concentration surrounded by dilute flow with a low solid concentration. These dense clusters are unstable as they continuously deform through complex transport mechanisms.

Decreasing the air velocity below the MCAV at a constant solids mass flow rate will further magnify the flow instabilities as dense clusters expand along the pipeline. This instability magnification is also reflected in the pipeline inner wall pressure, as dense clusters restrict the surrounding dilute phase to flow through smaller cross-section areas that continuously change.

The flow patterns in the transition phase near the PMC are rich with complex nonlinear dynamics. These dynamics can quantitatively be explored using high-dimensional phase spaces (attractors) reconstructed from time-series state measurements using the time-delay coordinate embedding method [8]. A phase space reconstructed from one state measurement of a system can reveal an equivalent topology to the system state space. The topological feature of reconstructed phase space can be described using statistical measures that, if captured correctly, can stay invariant across similar future topologies, including fractal dimension, Lyapunov exponent and entropy [9]. The fractal dimension is a measure of self-similarity that can be calculated using the Hurst exponent for a 1D time-series signal and the correlation dimension (CD) for an attractor. The chaotic behaviour of an attractor can be quantified using the largest Lyapunov exponent (LE), reflecting the separation of dynamics in each dimension of the phase space. The entropy of an attractor is the measure of the information generation rate of recurring dynamics involving both chaotic and stochastic dynamics, such as the Kolmogorov entropy [10] and the approximate entropy (AE) [11]. The recurring dynamics in an attractor can be visually observed in the recurrence plot (RP) initially introduced by Eckmann et al. [12], and its morphology is quantified using the recurrence quantification analysis (RQA) [13].

Considerable efforts have been made to characterise the complex dynamics of gas-solid flow patterns in horizontal pneumatic conveying systems through visual observation of 2D and 3D phase space reconstructed from pressure time-series signals [14–16]. Cabrejos and Klinzing analysed a 2D phase space qualitative behaviour of pressure signals using visual observation of their features at different flow patterns identified in horizontal pneumatic conveying systems [14]. This study stated that the pressure signals showed different global topological features in phase space for plastic pellets as the operating conditions

changed. Pahk studied the effect of a blower and feeder on a 2D phase space reconstructed from pressure signals in a horizontal pipeline using plastic pellets, which also follow the same phase space description provided by Pahk and Klinzing in ref. [15]. Later, Shijo studied the effect of solid loading ratio on pressure signals at different locations in a horizontal pipeline system using fly ash, a fluidised dense phase capable material [16]. In this study, the change in the flow from dilute to dense phase is captured in 3D phase spaces reconstructed from pressure signals acquired at different locations across a 120 m long pipeline.

The complex dynamics of gas-solid flow in fluidised bed systems have been extensively studied using chaotic invariants [17–21] and RQA measures [22–24] to monitor and identify operating conditions where the transition between different flow patterns occurs. In contrast, few studies aim to quantify the complex dynamics of gas-solid flow using chaos and RQA in pneumatic conveying systems. Cabrejos and Klinzing [25] studied the fractal dimension of a gas-solid flow pattern utilizing the Hurst exponent from pressure signals in a horizontal pneumatic conveying system at different operating conditions, indicating that the dilute phase has higher fractal complexity than the dense phase. Wang et al. used the Hurst exponent as a multiscale selection criterion for particle random energy ratio to identify the operating point at which the transition between suspension and deposition of solids occurs, found to be at the PMC [26]. Fu et al. characterised gas-solid flow dynamics in a vertical pneumatic conveying system of fine pulverized coal using the approximate entropy measure from electrostatic signals as a measure of solid concentration to distinguish dilute from dense phase flow operations [27]. The approximate entropy of electrostatic signals is found higher in the dense phase than in the dilute phase flow operation.

Although a phase space reconstructed from one time-series state of a system might reflect topological equivalence to the system state space. Specific states in the system can correlate more to the source of nonlinearity than others. Therefore, measurements from pressure and electrostatic sensor signals of a fully developed gas-solid flow are monitored in a horizontal pipeline system to compare the relationship of their nonlinear analysis measures with the operating conditions and observed flow patterns. The advantage of monitoring pressure and electrostatic sensors signals is that they are non-intrusive, low cost and relatively easy to implement in an industrial setting compared to other techniques that can provide direct measurements of local and global behaviour but are very costly to implement and have practical limitations, such as electrical capacitance tomography [28], phase-doppler

anemometry [29] and particle image velocimetry [30].

This paper aims to develop nonlinear time-series analysis, including chaotic invariants and RQA measures to characterise gas-solid flow behaviour and classify transition phase flow patterns near the PMC in an industrial-scale pneumatic conveying system. The analysis parameters settings are estimated using a heuristic procedure or set to a constant to be used as real-time flow pattern indicators, allowing the system to be operated at optimal conditions at the PMC.

2. Experimental setup

Experimental tests have been conducted in a close-loop industrial-scale pneumatic conveying system to capture fully developed gas-solid flow behaviour in a horizontal pipeline. Fig. 1 shows a schematic of the industrial-scale pneumatic conveying system and its main components. The main components of the pneumatic conveying system consist of a 0.1 m inner diameter pipeline with a total length of 127 m, receiving hopper and blow tank with a 1.5 m^3, a screw feeder, and a nozzle bank. In the loop, there are eight bends and two vertical pipeline sections. The loop consists of horizontal pipeline sections except for the sections before the second bend and after the last bend. Two screw-type compressors are used to compress air in tanks, which is then regulated and introduced in the pipeline cycle from the blow tank to receiving hopper using the nozzle bank at two locations: the blow tank exit, also known as 'blow tank air' (the screw feeder inlet), and the pipeline inlet also known as 'supplementary air' (the screw feeder outlet). The blow tank and supplementary air ratio can be adjusted per the requirement. Particulate materials are first fed to the blow tank through the feed hopper, then the blow tank is pressurised, and material is fed to the pipeline through a screw feeder using the blow tank and supplementary airflow. The air is separated from solids at the receiving hopper through a bag filter house with a surface area of 35 m^2.

The receiving hopper is suspended on three equidistant load cells. The load cells are manufactured by LCM SYSTEM LTS (STA-3-1000) with a range of up to 1000 kg and an accuracy of up to ±0.02%. The solids mass flow rate is measured using load cells and controlled by choosing a suitable air ratio between the blow tank and supplementary air and screw feeder motor speed. The m_a at the inlet of the pneumatic conveying pipeline system is controlled using the nozzle bank. The nozzle bank can incrementally control the m_a at the blow tank exit and pipeline inlet using different combinations of nozzles for each set, each
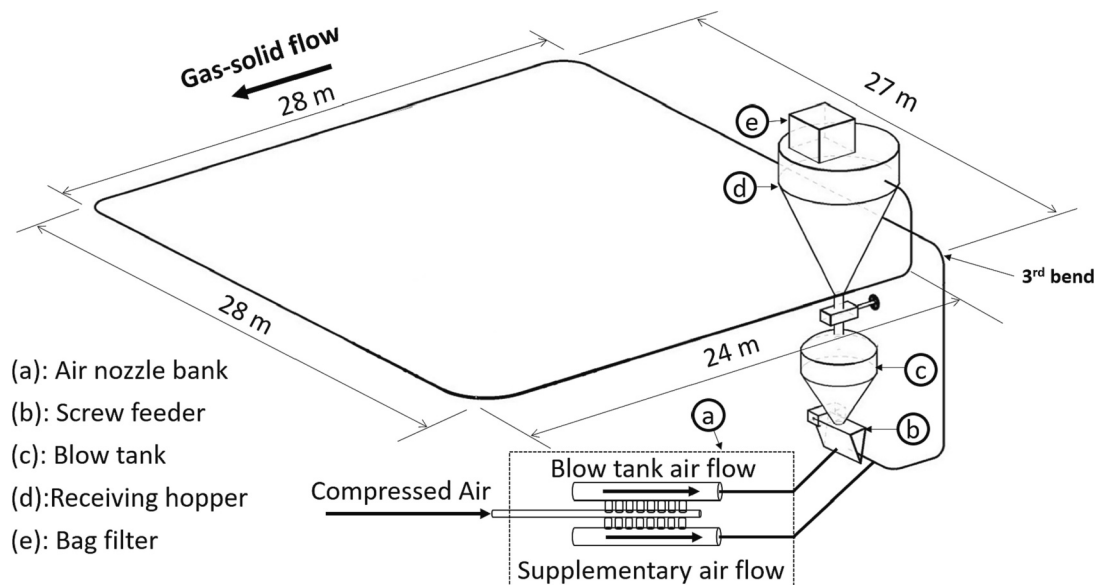

Fig. 1. A schematic of a pneumatic conveying system set up at The Wolfson Centre laboratory used to study the fully developed gas-solid flows in the horizontal pipeline downstream of the third bend.

with a maximum limit of 0.38 kg/s. The mass flow rate of air is set by combining several different sizes of choked flow nozzles with fixed upstream pressure, which delivers fixed mass flow rates of air irrespective of the downstream pressure up to a certain critical pressure ratio. The nozzle bank consists of two sets of eight nozzles each. The nozzle diameters range from 1.19 mm to 13.45 mm, with convergent-parallel-divergent sections having a critical pressure ratio of 80% (absolute pressures) across the nozzles. They operate with an upstream pressure of 62 kPa, meaning that provided the conveying pressure is below 52 kPa, the mass flow rate of air is fixed no matter how the conveying pressure changes. The nozzle bank was developed in The Wolfson Centre, further details on its dimensions and instrumentation and also its calibration can be found in Bradley (1990) [31].

Pressure measurements of gas-solid flow are undertaken using eight pressure transducers manufactured by DRUCK LTD (UNIK 5000), with measurements ranging up to 50 kPa and accuracy up to $\pm 0.04\%$. The first pressure sensor is installed 8 m downstream of the third bend to ensure gas-solid flow is transitioned from accelerating to fully developed. The first set of four pressure sensors is installed equidistantly with a 2 m separation distance, while the second set of four pressure sensors is installed 4 m after the fourth sensor with an equidistance of 2 m. The Wolfson Centre has developed the top and bottom arc-shaped electrostatic sensors assembly to measure qualitatively solids concentration and average velocity of charged particles [32]. The primary source of electrostatic charge developed on the solid particles is due to collisional friction between particles and the surrounding pipeline's inner wall, continuously going through positive and negative charges with a bimodal distribution. If fully charged particles pass through the 100% sensitivity zone (bottom section of the pipeline cross-section), the voltage signal will have high magnitudes and then return to zero and vice versa. The arc-shaped electrostatic sensors assembly is placed at 0.62 m from the first pressure sensor (P1), followed by a transparent pipeline to capture flow patterns using a high-speed video camera capturing images at 240 fps, as shown in Fig. 2.

Electrostatic signals were acquired from the bottom arc-shaped electrostatic electrode, which is amplified first using a transimpedance amplifier circuit with a measurement range from −5 to +5 V and then sampled with the first pressure sensor (P1) at 525 Hz. The Load cell and the rest of the pressure sensors from P2 to P8 are sampled at 1 Hz, sufficient for state diagram representation. LabVIEW software is used to acquire data, while the data analysis calculations are developed in MATLAB software.

A 2D grid of operating conditions is considered, including m_s and m_a, to study the effect of operating conditions on the flow patterns of plastic pellets observed in the transparent pipeline, pressure signal and bottom arc-shaped electrostatic signal. Ellipsoid shape plastic pellets with a total

batch mass of 800 kg are used, having a mean diameter of 3.6 mm, particle density of 910 kg/m^3 and bulk density of 560 kg/m^3. The m_a injected into the blow tank was kept constant throughout the transport process, and the screw feeder speed was set to five different incremental values. The m_s is calculated using a linear regression fit of the measured solids mass time-series signal in the fully developed flow region, as shown in Fig. 3 (a). The average pressure values from pressure sensors P1 to P8 are used to calculate the average pressure drop through a single regression fit across the eight sensors, as shown in Fig. 3 (b).

The initial experimental test point at constant screw feeder speed was conducted at a high supplementary m_a of 0.4 kg/s at the inlet of the transport pipeline to transport plastic pellets through dilute phase flow operation. Then the following test points were measured at the same screw feeder speed, and the supplementary air mass flow rate was progressively decreased by 0.02 kg/s using the nozzle bank until a single slug flow or settled layer appeared in the transparent pipeline. According to plug flow type capable materials, unstable flow in the form of slugs exists at an air velocity below the MCAV [5]. Therefore, further experiments are conducted at a constant m_s and progressively decreasing the m_a for each test to ensure that the transition flow spectrum between dilute and dense phase flow is captured using the installed sensors to identify the MCAV.

3. Analysis method

3.1. Phase space

Through time-delay coordinate embedding, one can reinflate a state variable from time-series measurements into a vector of latent state variables, assuming that the underlying dynamic is smooth with low-dimensional manifolds [8]. This method reconstructs a phase space from a time-series signal that exhibits topological equivalence to the original system state space. Reconstructing a phase space using the time-delay coordinate embedding method from measurements requires two main parameters - time delay and embedding dimension. Consider a signal $(x(t_1)...x(t_n))$, where n is number of points acquired at constant sampling periods. Eq. 1 shows the phase space data is in the form of a vector $Y(t)$ represented in the matrix form, where m is the embedding dimension, τ is the time delay, and N is the number of points in a phase space $(N = n - (m-1)\tau)$.

$$Y(t) = \begin{bmatrix} x(t_1) & x(t_{1+\tau}) & x(t_{1+2\tau}) & \cdots & x(t_{1+(m-1)\tau}) \\ x(t_2) & x(t_{2+\tau}) & x(t_{2+2\tau}) & \cdots & x(t_{2+(m-1)\tau}) \\ \vdots & \vdots & \vdots & \ddots & \vdots \\ x(t_N) & x(t_{N+\tau}) & x(t_{N+2\tau}) & \cdots & x(t_{N+(m-1)\tau}) \end{bmatrix} \quad (1)$$

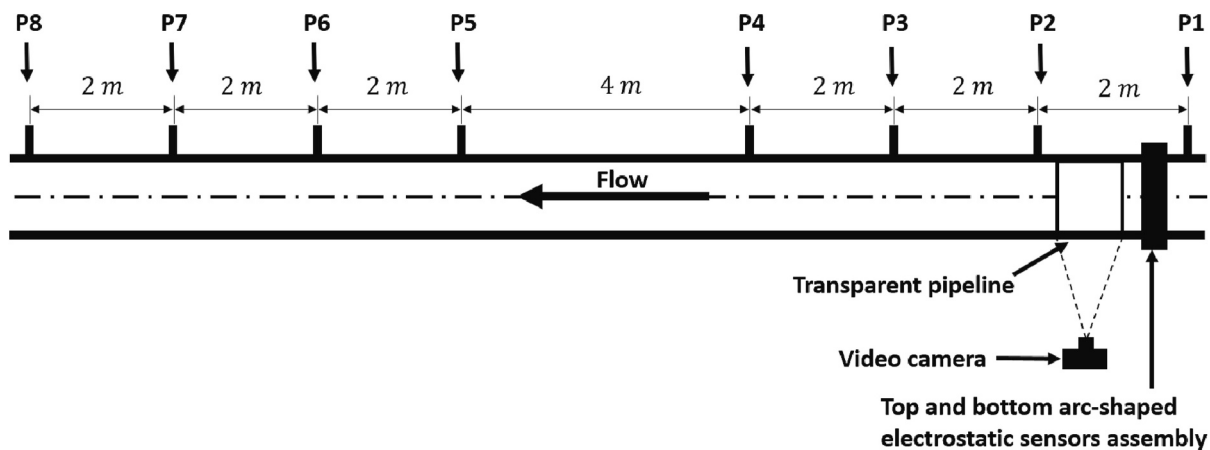When the dynamic complexity of a time series signal is steamed from

Fig. 2. A schematic diagram of the horizontal pipeline downstream of the third bend showing the location of the pressure sensors from P1 to P8 and the top and bottom arc-shaped electrostatic sensors assembly.
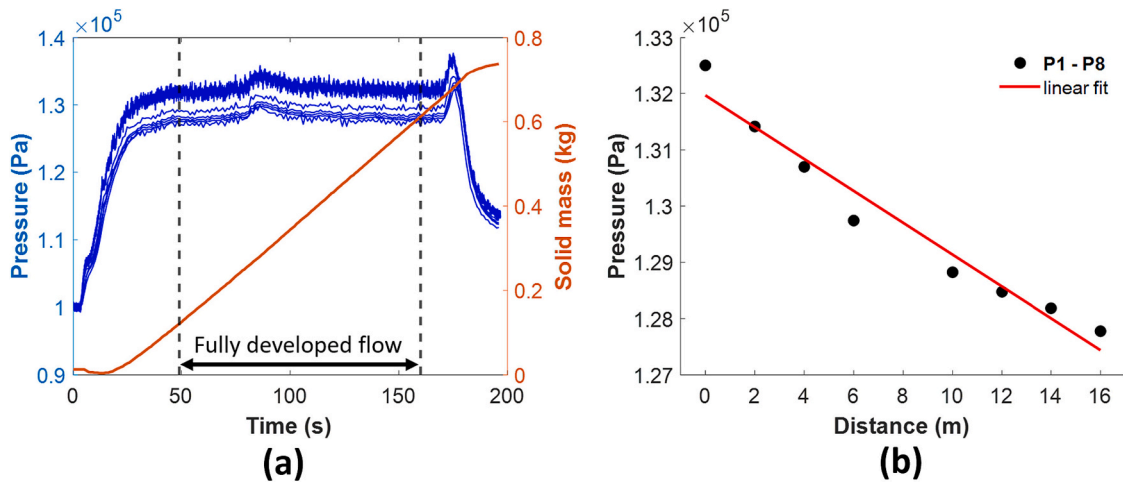
Fig. 3. (a) Pressure and load cell signals of plastic pellets acquired at $m_a = 0.26$ kg/s and $m_s = 3.8$ kg/s. (b) The average pressure for each signal versus their distances from the first pressure sensor location and the linear regression for the pressure drop.

a stochastic dynamical system, its reconstructed attractor will correspond to infinite-dimensional space with no meaningful information. The false nearest neighbour Algorithm (FNN) is a commonly used algorithm to estimate the embedding dimension of a signal, which is based on the idea that if not enough dimension is used to unfold the dynamics, there will be trajectory crossings in the dynamics [33]. These crossings are noise caused by high to low dimensional space projection. This algorithm scans for trajectory crossings by distinguishing true neighbouring points from false ones for an attractor while increasing the embedding dimension, as shown in Eq. 2.

$$\sqrt{\frac{R_i(m+1) - R_i(m)}{R_i(m)}} > D, R_i(m) = \|Y_i - Y_s\|^2 \qquad (2)$$

$R_i(m)$ is the distance between phase point Y_i and their nearest neighbour point Y_s, where $i = 1 : N$ and D is the distance threshold to identify false neighbours. The embedding dimension is selected based on a satisfied condition of false neighbour percentage, which is the ratio of FNN points to the total number of points in the reconstructed phase space.

3.2. Chaotic invariant measures

Fractal dimension is a measure that characterises patterns in an attractor through self-similarity, quantified using a scaling function that correlates a change in geometrical detail to a change in scale. Several methods for calculating the fractal dimensions are used, such as capacity dimension (box counting), correlation dimension, and Hausdorff dimension. The calculation of the correlation dimension is the quickest and subjected to less noise when not enough points in the attractor are available. The correlation dimension (CD) calculation algorithm was initially developed by Grassberger and Procaccia [34] and then modified by Theiler [35] to speed up the calculation a thousand times more. The CD is calculated through linear regression in a region of interest in the correlation integral function (Cr) in the log scale (log(Cr)), a function of scaled hypersphere similarity radius (r). Cr in an attractor corresponds to the sum of nearby trajectory points within r from a template trajectory of the attractor. Eq. 3 shows the Cr(r) function, where $\|X_i - X_j\|$ is the vector distance between phase points and Θ is the Heaviside step function presented in Eq. 4.

$$Cr(r) = \frac{2}{N(N-1)} \sum_{i=1}^{N} \sum_{j \neq i}^{N} \Theta\left(r - \|Y_i - Y_j\|\right) \qquad (3)$$

$$\Theta = \begin{cases} 1 \ h \geq 0 \\ 0 \ h < 0 \end{cases} \qquad (4)$$

The sensitivity of initial conditions is a natural phenomenon that describes chaotic behaviour, quantified using the Lyapunov exponent. Lyapunov exponent characterises the separation rate between two neighbouring trajectories in state space. There are as many Lyapunov exponents as there are dimensions known as the Lyapunov spectrum, which correspond to each separation direction in a system state space. If all the Lyapunov exponents of an attractor are negative, all trajectories are shrinking from all directions toward stable manifolds. If all Lyapunov exponents are positive, then trajectories diverge in unstable manifolds. To have an attractor means the sum of all Lyapunov exponents tends to approach zero and negative for dissipative systems. For a chaotic attractor, there is at least one positive Lyapunov exponent. However, this cannot indicate whether an attractor is chaotic, as there will be a combination of stable and unstable manifolds. Typically, the positive Lyapunov exponent in a set of initial conditions dominates growth in an attractor in the long run.

In this study, only the largest Lyapunov exponents (LE) are used to measure chaotic behaviour in a time series. The algorithm for the LE is adopted from Rosenstein [36]. Lyapunov exponent $\lambda(i)$ is a function of phase point i across the expansion step k, presented in Eq. 5. The value of k_{min} and k_{max} are the minimum and maximum values of the expansion range. Where $\|Y_i - Y_s\|$ is the distance between each phase point i and its nearest neighbour s and $\|Y_{i+k} - Y_{s+k}\|$ is the change after an expansion step k. The nearest neighbour points in this algorithm satisfy the condition $|i - s|\rangle minimum\ separation$. The minimum separation is calculated using the ratio of the sampling frequency of the signal to its mean frequency, allowing enough space for initial conditions from neighbouring trajectories of interest to be considered. For each expansion step, one value of the Lyapunov exponent is calculated using the average of positive Lyapunov exponents for all the phase points, also called average log divergence (ALDiv). Across the expansion steps from k_{min} and k_{max}, a single value for the Lyapunov exponent is calculated through linear regression fit across an expansion range of interest. A phase space with positive LE indicates that the dominant structure is chaotic, negative LE indicates dissipative nature and zero LE represents periodic or fixed points.

$$\lambda(i) = \frac{1}{k_{max} - k_{min} + 1} \sum_{k=k_{min}}^{k_{max}} \frac{1}{k \times dt} ln \frac{\|Y_{i+k} - Y_{s+k}\|}{\|Y_i - Y_s\|} \qquad (5)$$

Pincus developed the approximate entropy measure, a modification of Kolmogrov-sini entropy, featured by its low computational cost and

capability to deal with noisy data [11]. Approximate entropy (AE) reflects the logarithmic probability of the degree of unpredictability of future information based on previous similar information. The AE has a self-counting feature that compares the closeness of trajectory points in an attractor with other older points. Zero AE corresponds to constant or cyclic behaviour, represented in phase space by a fixed point or periodic attractor. AE is calculated by subtracting two statistical functions; Φ_m from Φ_{m+1}, as shown in Eqs. 6 and 7, computed using a phase space reconstructed with the selected dimension m and at a higher dimension $m + 1$.

$$AE = \Phi_m - \Phi_{m+1} \tag{6}$$

$$\Phi_m = \frac{1}{N} \sum_{i=1}^{N} log \left(\sum_{j=1, j \neq i}^{N} \Theta \left(r - \left\| Y_i - Y_j \right\| \right) \right) \tag{7}$$

3.3. Recurrence plot

The recurrence plot (RP) is a representation of the dynamic topology of an attractor, developed by Eckmann et al. in 1987 as a visualisation tool that projects recurring dynamics from high dimensional phase space into a 2D black and white (binary values) plot [37]. It reflects the process of having trajectory points in phase space arbitrarily visiting each other at different times. $RP_{i,j}$ in Eq. 8 is a square matrix relating pairs of times at which phase points meet in a fixed hypersphere with radius r. The subscript i and j are the index of the matrix for each pair of phase points. $\left\| \overrightarrow{Y}_i - \overrightarrow{Y}_j \right\|$ Y is the matrix of the global RP, representing the distances between pair of points in an attractor. The distribution of recurrent points in RPs heavily depends on the selected threshold r. However, the r threshold selection is less critical for comparative studies of dynamical transitions, as differences between RP would not change within a specific distance range.

$$RP_{i,j}(r) = \Theta \left(r - \left\| \overrightarrow{Y}_i - \overrightarrow{Y}_j \right\| \right) \tag{8}$$

RPs have a main diagonal line that is black, separating two identical triangles, known as the line of identity (LOI). Marwan et al. [38] described several qualitative structures of black points around the LOI. The identical triangles contain a geometric arrangement of recurrent points, denoted as typology by Eckmann et al. [37], capable of revealing several global dynamic characteristics such as homogenous, periodic, drift and disruption. The homogenous structure represents a stationary time-series signal containing uniformly disrupted recurrent points, reflecting a random behaviour. The periodic structure has repeated dense local structures and long diagonal lines separated at equal distances, describing a cyclic process. For a quasiperiodic signal, diagonal lines have different distances between each other. The drift structure represents a non-stationary signal with slowly varying values, showing a low density of points around the LOI and white corners. The disruption structure is present when rare extreme events occur, appearing as broad white areas or bands in the RP.

Small-scale structures can also give different dynamic interpretations. Single isolated points mean the dynamic process does not persist or fluctuate randomly. Diagonal lines reflect similar dynamic evolution and appear when trajectories in an attractor are parallel. Trajectories evolve in the same direction if the diagonal lines are parallel to the LOI and perpendicular when they evolve in opposite directions. Discontinuous diagonal lines that appear periodically describe chaotic behaviour in an attractor as unstable periodic orbits separate parallel trajectories and converge them again. Vertical lines appear when trajectories stop or evolve slowly in specific locations in an attractor, describing intermittent behaviour.

The multiscale structure of RPs reconstructed from pressure signals describing gas-solid flow patterns in fluidized beds have been classified into two groups, local white areas (LWA) and local bolt areas (LBA) [22,39]. The LWA correspond to a macroscale structure in an attractor with trajectories with higher distances than the selected threshold r, reflecting high amplitudes and low-frequency dynamics. In contrast, the LBA represents mesoscale and microscale structure having trajectories separated with distances smaller than the threshold r, describing high-frequency dynamics.

3.4. Recurrence quantification analysis

RPs can reveal valuable qualitative information about the dynamic structure of attractors. Inspecting the recurrent points structure in RPs to detect slight variations in the dynamics is challenging, especially when there are multiscale recurrent structures. RQA quantifies structural complexity using numbers and durations of recurring dynamics in RPs. The RQA measures were initially developed by Zbilut and Webber [13] and Webber and Zbilut [40], using the recurrence density points and the length of diagonal lines. Measures based on diagonal lines can detect chaos-order transitions. Marwan et al. [41] extended the RQA with other descriptive measures calculated using vertical lines, revealing chaos-chaos transitions. Later, Marwan et al. (2007) provided more definitions and explanations of different RQA measures.

The RQA measures used in the analysis are recurrence rate (RR), determinism (DET), entropy (E) and average diagonal line length (L). The RR measure is the ratio of recurrent points to the total number of points, as shown in Eq. 9, which is related to the Cr function in CD estimation. The DET is the percentage of diagonal lines of recurrent points, presented in Eq. 10, where P(l) is the histogram of diagonal lines, and l_{min} is the minimum diagonal lines in a recurrence plot, typically taken at $l_{min} = 2$ [42]. The E measure is calculated based on Shannon entropy using the distribution of diagonal lines parallel to the LOI, as shown in Eq. 11. The L measure presented in Eq. 12 describes the deterministic process in an attractor by characterising the average duration at which trajectories evolving in the same direction in space are arbitrarily close to each other.

$$RR = \frac{1}{N^2} \sum_{i=1}^{N} \sum_{j=1}^{N} R_{i,j} \tag{9}$$

$$DET = \frac{\sum_{l=l_{min}}^{N} l \times P(l)}{\sum_{l=1}^{N} l \times P(l)} \tag{10}$$

$$E = \sum_{l=l_{min}}^{N} P(l) \times ln(P(l)) \tag{11}$$

$$L = \frac{\sum_{l=l_{min}}^{N} l \times P(l)}{\sum_{l=l_{min}}^{N} P(l)} \tag{12}$$

4. Results and discussions

4.1. Flow pattern map and state diagram

Coarse solid particles like plastic pellets with a mean diameter >1 mm are expected to be conveyed at the MCAV without blockages [43]. Tsuji studied the wall pressure fluctuation of horizontal gas-solid flows of plastic pellets with $d_{50} = 2.3\ mm$ and observed its flow patterns close to the PMC, describing them as sliding dense clusters [44]. Cabrejos provided more generalised descriptions of horizontal gas-solid flow patterns and their relations to the operating conditions using three materials with different material properties [14]. The flow patterns identified for plastic pellets with $d_{50} = 3\ mm$ are homogenous flow,
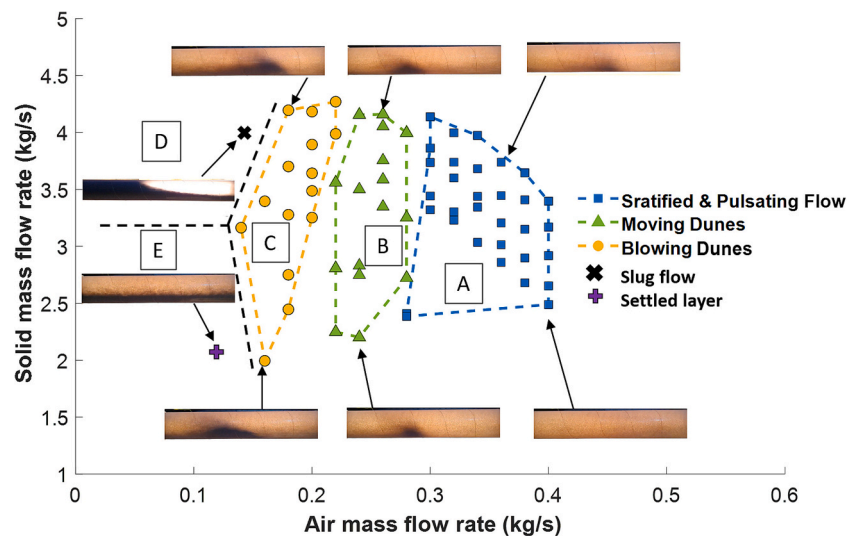
Fig. 4. The flow pattern map for horizontal pneumatic conveying of plastic pellets.

stratified flow, pulsating flow, moving dunes and blowing dunes.

The flow pattern map illustrates the formation of gas-solid flow patterns at different operating conditions. It is a scatter of operating points, including m_s and m_a, classified into regions identified based on the flow pattern observed in a transparent pipeline. Fig. 4 shows the flow pattern map for horizontal pneumatic conveying of plastic pellets classified into three patterns: stratified/pulsating flow, moving dunes and blowing dunes. The regions of these flow patterns vary across different m_s and m_a. Beyond the left boundary, slug flow (region D) and settled layer (region E) are present in the upper and lower regions.

At a high m_a of 0.4 kg/s and low m_s of 2.48 kg/s (lower boundary of region A), plastic pellets are in suspension mode, where particles are distributed across the pipeline cross-section with high solids concentration at the lower section of the pipeline, namely stratified flow. At the same m_a but higher solids mass flow rate of 3.4 kg/s (lower to the upper boundary in region A), plastic pellets are in an intense kinetic and frictional collision as they accumulate and form discontinuous clouds at the bottom of the pipeline, known as pulsating flow. As the m_a reduces at a particular point (transition from region A to B), which is 0.28 kg/s in this case, self-organised critical states appear as moving dunes surrounded by dilute phase sliding on the bottom of the pipe. Moving dunes are featured by continuous erosion at the up-wind side (luff) and deposition at the down-wind side (lee). With further reduction in m_a, solid particles in dilute phase flow start to drop out of suspension, and multiple moving dunes slow down and merge, forming blowing dunes. At the left boundary of blowing dunes, dunes start to settle down, and the transportation mechanism starts to be dominated by saltation and surface creep. Beyond this boundary, plug flow (region (E)) and settled layer (region (D)) at the upper and lower regions are present.

Fig. 5 shows a state diagram developed using the data gathered from the horizontal pneumatic conveying of the plastic particles. Each solids mass flow rate is included for each point through a colour spectrum referring to the colour bar values, and the flow patterns are classified into regions. The superficial velocity is calculated based on the mean pressure and pipe diameter using the ideal gas law at ambient temperature and plotted as a function of the pressure drop per unit length of pipe. Correlating pipeline pressure drop with gas-solid flow patterns reveals how specific flow patterns influence the pressure drop. The PMC is present between the moving dunes and the blowing dunes regions, where the transport mechanism is dominated by sliding, erosion and deposition of particles.

4.2. Analysis parameters settings

The top air-wall pressure and bottom arc-shaped electrostatic signals from three air velocities 33.5 m/s, 20 m/s and 16 m/s at low solids mass flow rates $m_s = 2.6$ kg/s, 2.2 kg/s and 2.5 kg/s representing the stratified flow, moving dunes and blowing dunes are used as a template to show the analysis parameters settings. Chaotic invariants and RQA calculations are applied to phase spaces reconstructed from a 1 s moving time window of data (525 data points) with an overlap of half of the time window size (262 data points) for a total of 30s (15,750 data points). The phase spaces are reconstructed using a time delay of 1, and the embedding dimension is estimated using FNN. The recommended heuristic for FNN parameters is to select an embedding dimension that satisfies 10% of false neighbours. The number of false neighbours is determined at a distance threshold of 1. The dimensions are estimated for the moving time window of pressure and electrostatic signals. The pressure data dimensions vary between 8 and 10, and electrostatic data vary between 9 and 13. Dimensions 9 and 10 are the shared value between the pressure and electrostatic signals. Therefore, the choice of the dimension used to reconstruct phase spaces and develop recurrence plots for the moving time window is 10.

Calculating a single LE requires linear regression across an expansion range in the ALDiv function. Fig. 6 presents ALDiv as a function of an incremental expansion time step for phase spaces reconstructed from
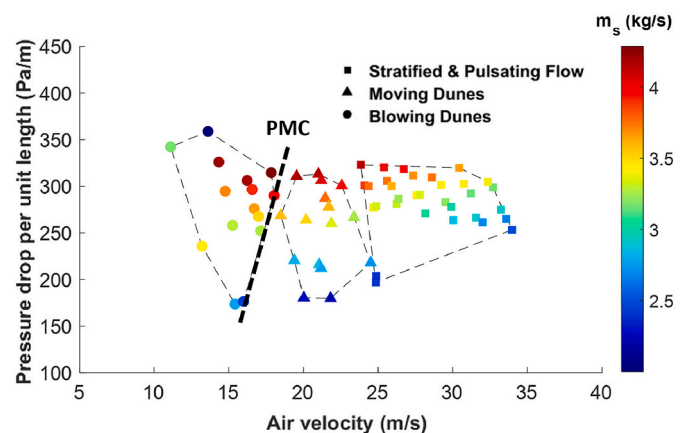

Fig. 5. State diagram for horizontal pneumatic conveying of plastic pellets with classified flow patterns regions.
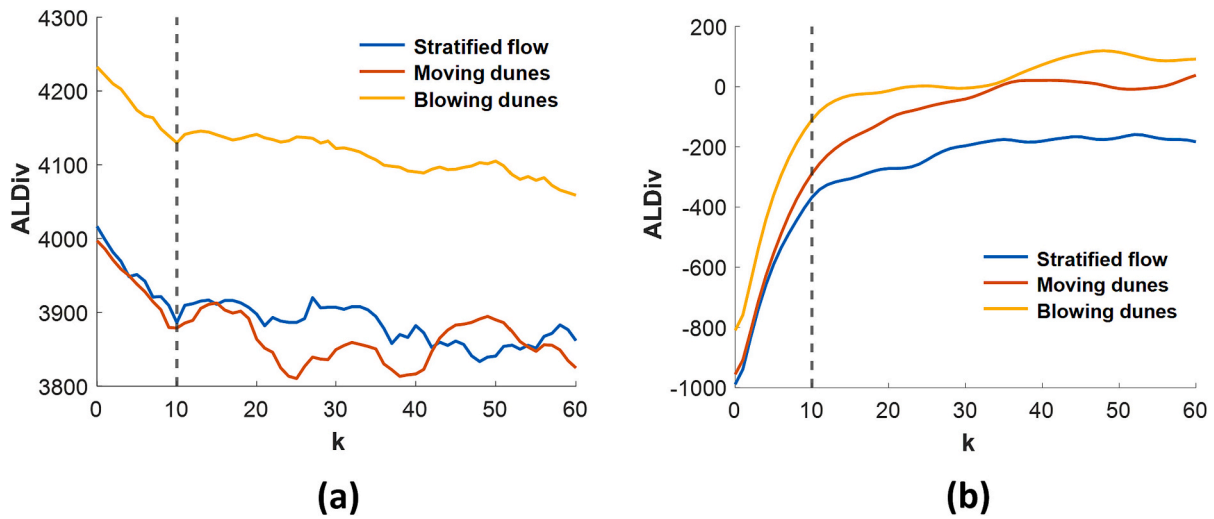
Fig. 6. An average log divergence vs expansion step for (a) pressure signals and (b) bottom arc-shaped electrostatic signals acquired at air velocities of 33.5 m/s, 20 m/s and 16 m/s and m_s = 2.6 kg/s, 2.2 kg/s and 2.5 kg/s representing the stratified flow, moving dunes and blowing dunes respectively.

pressure and electrostatic signals under different operating conditions. The initial trends of ALDiv for phase spaces reconstructed from pressure signals are a linear decrease indicating that it is dissipative (negative LE), and phase spaces reconstructed from electrostatic signals are a linear increase reflecting chaotic behaviour (positive LE). The trend then shifts to a relatively constant value at a specific expansion step. The expansion range used to estimate LE for the moving time window is between 1 and 10 across all operating conditions.

AE is the probability that future similar trajectories, including stochastic and deterministic, do not follow past similar trajectories. The parameter required to calculate the AE of an attractor is the threshold r. The chance that trajectory points in an attractor have other points than itself falling within a hypersphere with a small r (r_1) is zero or very low. As r increases, more trajectory points are included in determining the probability between future and past similar dynamics. A typical distribution of AE across r is an increase in the unpredictability of information up to a specific r, forming the most significant difference between past and future information. The distribution of AE beyond this particular r gradually decreases to zero as the relation between future information becomes regular to the past information, and r approaches the maximum

value between the points. It is recommended to select r within the range of 0.1 to 0.2 times the standard deviation of the signal. Sometimes the standard deviation approach may lead to an incorrect assessment of the signal complexity [45]. A more appropriate approach is to select the maximum value of AE (AE_{max}) across r or an AE at a slightly higher r than the r at AE_{max} (r_{AEmax}) to avoid misleading comparative results [46]. The AE values shown in Fig. 7 (a) and Fig. 7 (b) are calculated at 50 equidistant r across the phase spaces reconstructed from pressure and electrostatic signals to identify r_{AEmax} and select AE_{max}.

The CD measure is calculated through linear regression of the Cr function in a scaling region of interest that exhibits self-similar fractal geometry. For a mono-fractal attractor, the r scaling region is located between depopulation and saturation regions at the low and high ends of the r scales [47]. Fig. 8 shows the Cr at different r for pressure and electrostatic signal phase spaces, reflecting a mono-fractal geometry as there is only one linear scaling region across r. The scaling region's first r (r_{Cr1}) and second r (r_{Cr2}) are automatically selected based on the distribution of AE across r. As r_{AEmax} represents the shift point between high to low unpredictability of information, it will be the same as r_{Cr1}. While r_{Cr2} is selected with the condition that it should have zero AE and be
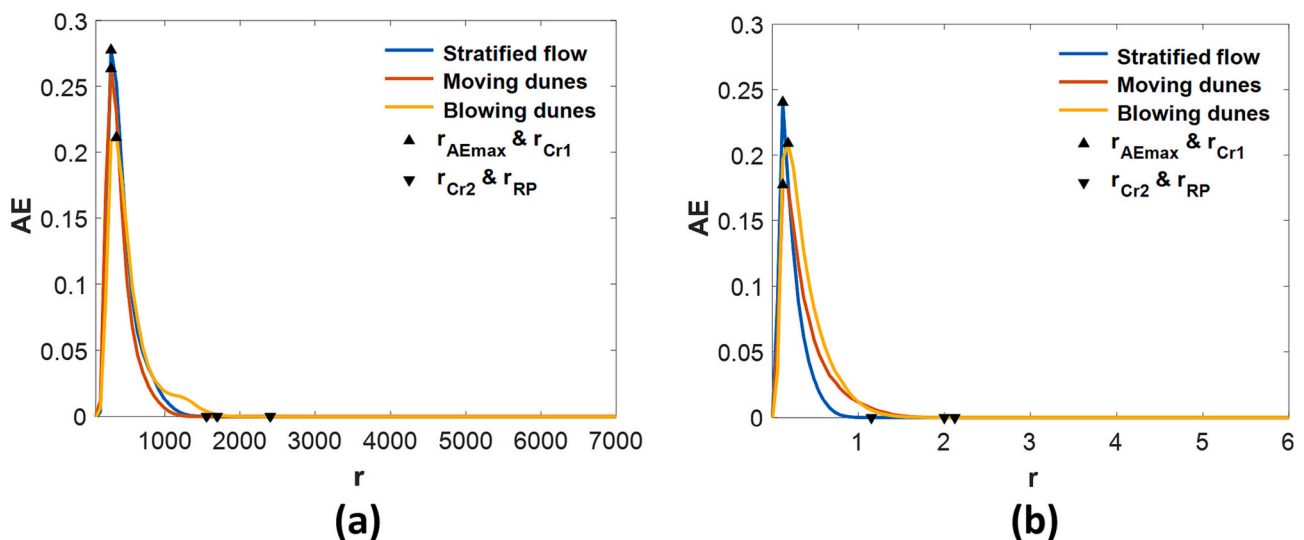

Fig. 7. An approximate entropy vs radius for (a) pressure signals and (b) bottom arc-shaped electrostatic signals acquired at air velocities 33.5 m/s, 20 m/s and 16 m/s and m_s = 2.6 kg/s, 2.2 kg/s and 2.5 kg/s representing the stratified flow, moving dunes and blowing dunes respectively.
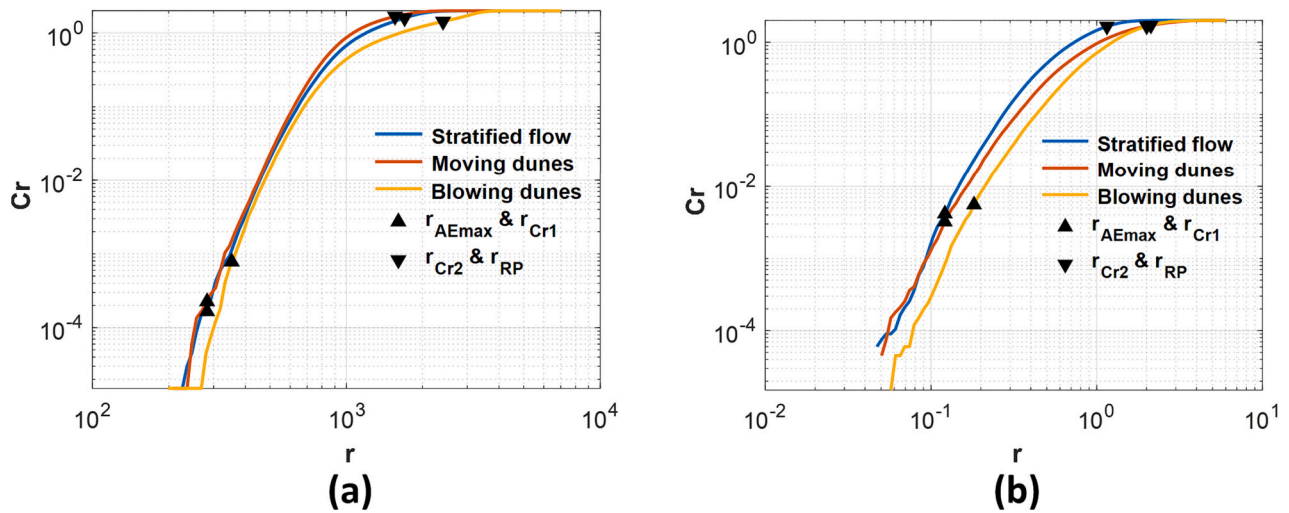
Fig. 8. A Cr vs r for (a) pressure signals and (b) bottom arc-shaped electrostatic signals acquired at air velocities of 33.5 m/s, 20 m/s and 16 m/s and m_s = 2.6 kg/s, 2.2 kg/s and 2.5 kg/s representing the stratified flow, moving dunes and blowing dunes respectively.

higher than r_{Cr1} to focus on the CD measure that has a high probability of regularity between past and future dynamics.

Extracting meaningful measures from RPs using the RQA requires an appropriate threshold r (r_{RP}) depending on the application type [48]. Initial rule of thumb choices for r_{RP} are taken at 10% of the maximum diameter of phase space or 5% of the mean diameter [13] or a threshold r at 1% recurrence rate [49]. Using the recurrent diagonal structures parallel to the LOI in RPs was appropriate for optimal threshold selection for quasiperiodic systems [50]. Later Gao and Jin [51] presented a criterion for selecting the optimum threshold using the first maximum value of the derivative of the recurrence rate with respect to the r (dRR/dr). However, the r at the first maximum value of dRR/dr can be impractical when there are multiple maxima across r, clearly observed in quasiperiodic systems [52]. This issue can be observed in Fig. 9 for the dRR/dr of pressure signals, showing multiple local maxima which change across different time windows. While for electrostatic signals, only one maximum is observed across different time windows. Instead of looking at the dRR/dr to select the threshold r, AE is used to have more consistent RQA measures. Instead, the r_{RP} value is set to be the same as r_{Cr2} to ensure that the RPs will have a high probability of predictable dynamics in the RPs.

4.3. Recurrence plots

Fig. 10 to Fig. 11 show 30s of normalised pressure and 1 s of bottom arc-shaped electrostatic signals and their recurrence plots (RPs) for different air velocities 33.5 m/s, 20 m/s and 16 m/s at low solids mass flow rates m_s = 2.6 kg/s, 2.2 kg/s and 2.5 kg/s. The RPs have different structured distributions of recurrent points for different flow patterns, including the stratified flow, the moving dunes and near the blowing dunes transition to the settled layer. These distributions reveal various local white areas (LWA) and local bolt areas (LBA), providing qualitative information on pressure signals and electrostatic signal fluctuations. The LWA of RPs developed from pressure signals in a fluidized bed system was found by Babaei et al. [39] to be related to macroscale behaviour such as air bubble formation, fluidization column and air impulsion equipment. In contrast, the LBA reflected mesoscale and microscale behaviours describing interactions of small air bubbles, dense clusters of solid particles and individual solid particles. The nature of pressure fluctuations caused by specific material depends on the source of its origin, which can be affected by pneumatic conveying system equipment and operating conditions. Nevertheless, relative influences of operating conditions on the RPs structures from pressure and electrostatic signals can be observed through the change in the LWA and the LBA.
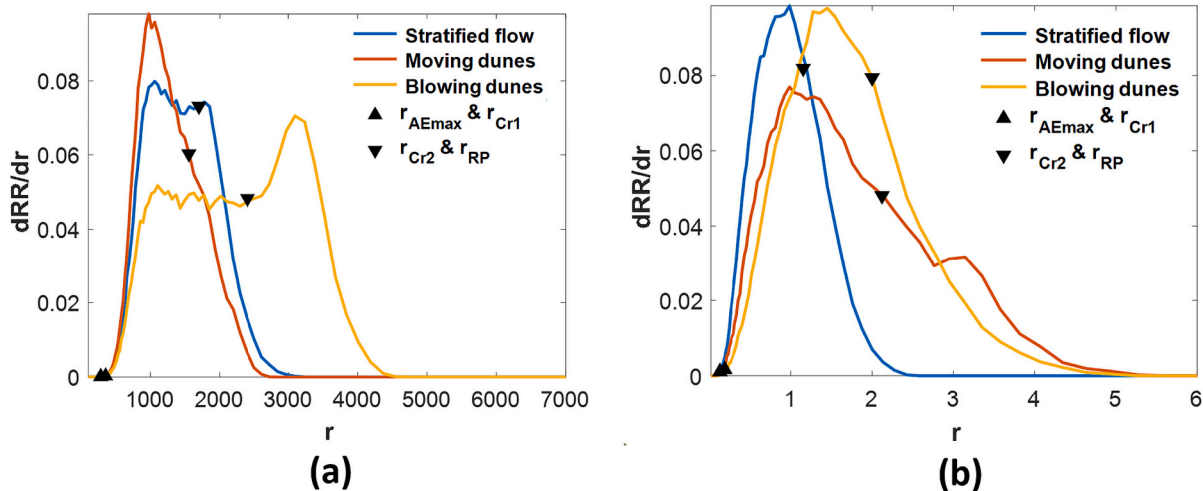

Fig. 9. A derivative of recurrence rate radius vs radius for (a) pressure signals and (b) bottom arc-shaped electrostatic signals acquired at 33.5 m/s, 20 m/s and 16 m/s and m_s = 2.6 kg/s, 2.2 kg/s and 2.5 kg/s representing the stratified flow, moving dunes and blowing dunes respectively.
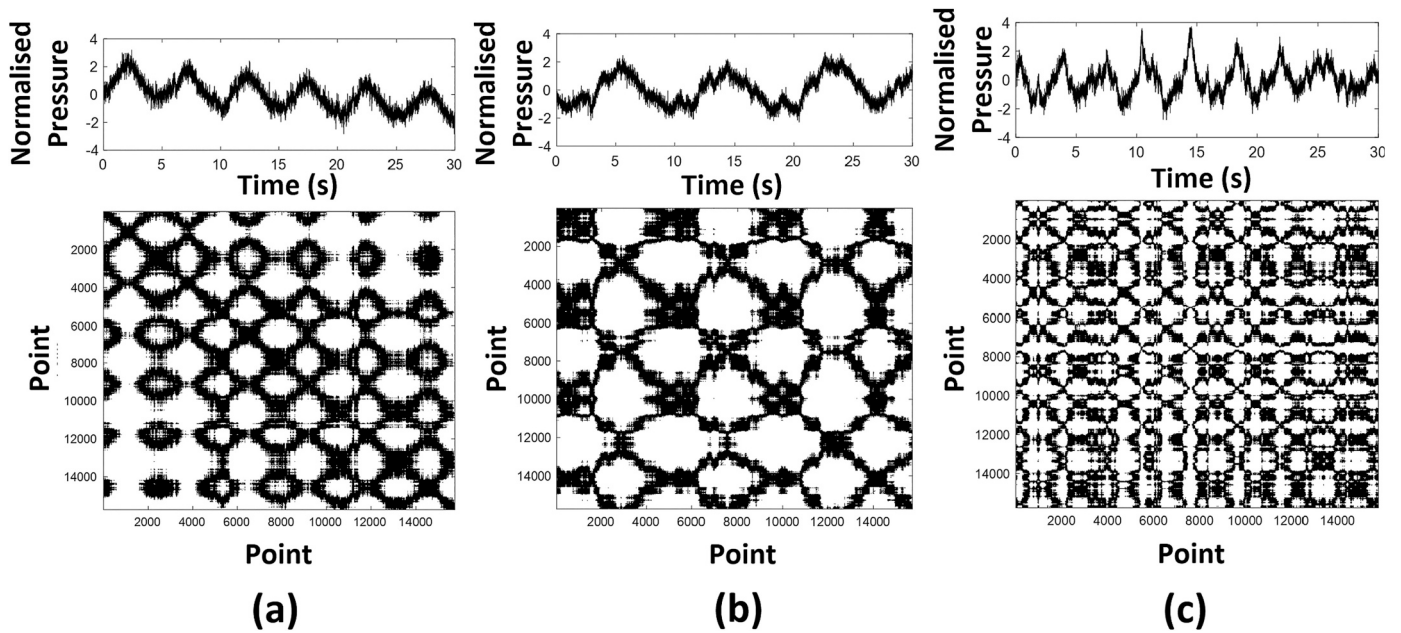
Fig. 10. Recurrence plot developed from pressure signals for (a) stratified flow, (b) moving dunes and (c) blowing dunes transitioning to settling layer at air velocities 33.5 m/s, 20 m/s and 16 m/s and m_s = 2.6 kg/s, 2.2 kg/s and 2.5 kg/s.

The RPs reconstructed from pressure signals in Fig. 10 (a), (b) and (c) show dissipative structures with decreasing LWA values and, consequently, LBA increases, evolving from stratified flow to blowing dunes. Although the LWA increases, their occurrence and irregularity increase, meaning that the disruptions are due to more frequent but rare extreme events occurring in pressure signals. In stratified flow, individual plastic pellets are in suspension mode and are dispersed with high solid concentrations at the bottom section of the pipeline, having minimal effect on the complexity of pressure signals. The pressure signal behaviour of stratified flow is periodic, observed in the RPs shown in Fig. 10(a), through the consistency of diagonal lines parallel to the LOI and repeated structure of LWA. As the flow evolves from stratified flow to moving dunes, as shown in Fig. 10(b), the thickness of the diagonal lines decreases and, in some instances, converges to thin lines.

The moving dunes flow pattern has more influence on the complexity of pressure fluctuations than stratified flow, which is caused by airflow
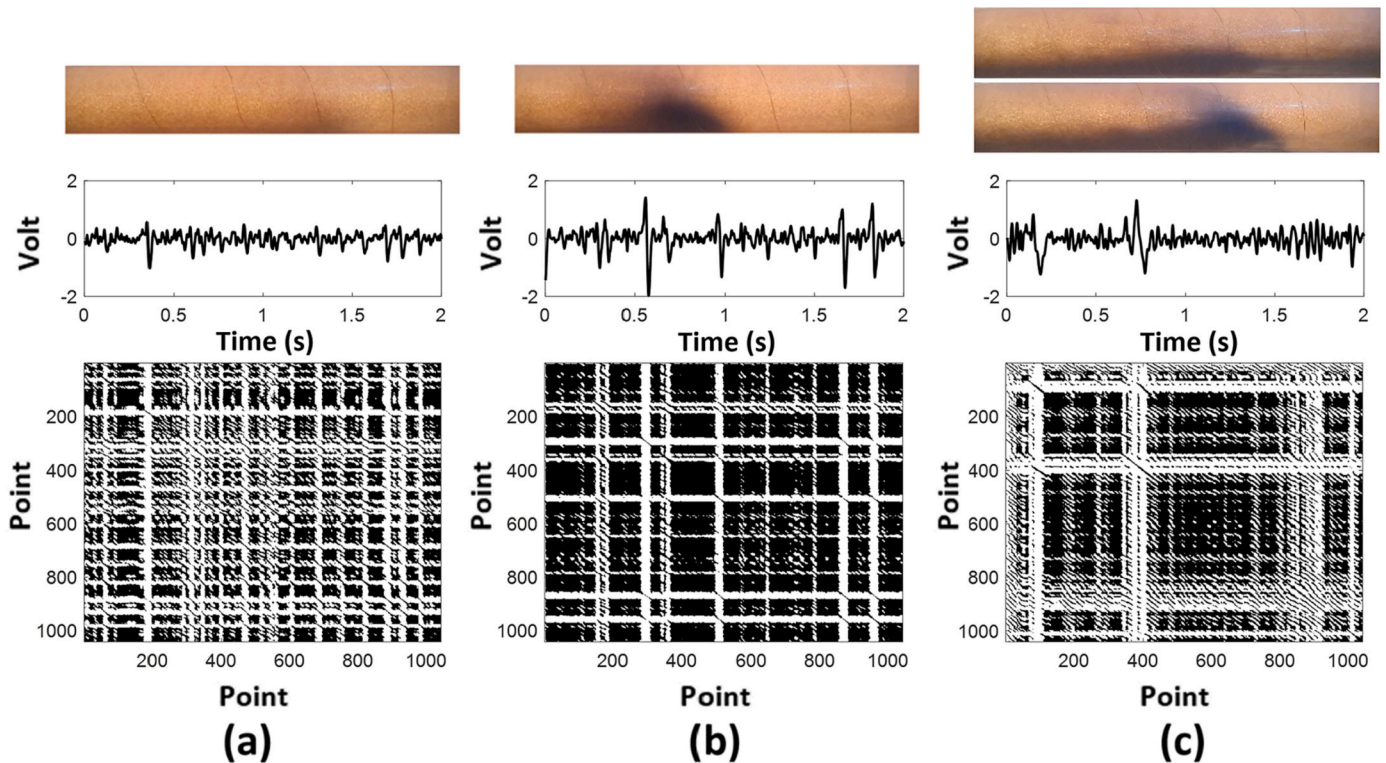

Fig. 11. Recurrence plot developed from bottom arc-shaped electrostatic signals for (a) stratified flow, (b) moving dunes and (c) blowing dunes transitioning to settling layer at air velocities 33.5 m/s, 20 m/s and 16 m/s and m_s = 2.6 kg/s, 2.2 kg/s and 2.5 kg/s.

redirections around and through the dunes creating high pressure in the luff and low pressure on the lee side of the dune. This complexity is magnified even further in blowing dunes as dunes size increases, forcing the air to flow through smaller areas. This event of high and low-pressure pulses around the dunes depends on its shape, size, and inter-action with the dispersed particles on top and the pipeline wall at the bottom. The chance of having these interactions repeated in a short period are rare, reflected in the increased number and complexity of LWA from stratified flow to blowing dunes, as shown in Fig. 10 (c).

The solid concentrations of charged particles and their arrangement across the pipeline bottom cross-section for each flow pattern have different effects on the voltage signal from the bottom arc-shaped electrostatic sensor, as shown in Fig. 11. These voltage signals are directly related to the charging capacity of particles and their location in the local sensitivity region of the sensor. The RPs of electrostatic signals in Fig. 11 show a much more complex structure of recurrence points than the RPs of pressure signals in terms of shortness of diagonal lines length and increased isolated LBA values. This difference indicates that electrostatic signals exhibit chaotic features and contain more stochastic behaviour than pressure signals. By comparing the LBA values in RPs from electrostatic signals across the flow patterns, it can be observed that it increases from stratified flow in Fig. 11 (a) to moving dunes in Fig. 11 (b). This increase in the LBA or decrease in the LWA indicates that the macroscale events in stratified/pulsating flow in relation to its overall dynamics are higher than moving dunes. This can be directly linked to a change in macroscopic flow patterns from charged particles in discontinuous clouds that appear more frequently when compared to moving dunes transported at lower air velocity, as shown in Fig. 11 (c).

In the evolution of gas-solid flow from moving dunes to blowing dunes, dispersed particles start to drop out of suspension, and moving dunes slow down and merge into more prominent dunes having more flexible structures that appear less frequently or into a settling layer. Although the event of accumulated solids appearance in blowing dunes transitioning to settled layer flow patterns will reappear less frequently, they appear for more extended periods than moving dunes and clouds, reflected in the increasing LWA values in the RPs of electrostatic sensor data from moving dunes in Fig. 11(b) to blowing dunes transitioning to settling layer in Fig. 11(c).

4.4. Nonlinear dynamics analysis measures

The gas-solid flow patterns in horizontal pneumatic conveying of plastic pellets have different complex dynamics, observed using the RP similarities of pressure and bottom arc-shaped electrostatic signals. The dynamic complexity of the 30s of pressure and electrostatic signals are quantitatively measured using chaotic invariants, including LE, AE and CD, and their similarity using RQA, including RR, DET, E and L, using the parameters settings mentioned in Section 4.2. Fig. 12 to Fig. 14 show profiles of the average values of the analysis measures across the moving time window, correlated with air velocity, pressure drop and the observed flow patterns in state diagrams.

Fig. 12 (a) and (b) shows the profile of LE across the operating conditions in the state diagram expressing the degree of chaotic behaviour in pressure and electrostatic signals. The LE values of elec-trostatic signals at constant solids mass flow rates and higher air ve-locities than the MCAV have an inverse relationship with the air velocity and pressure drop. The relationship between the LE values and pressure drop changes to a direct relationship at air velocities below the mini-mum conveying air velocity, where the highest LE values are localised at the blowing dunes flow pattern left boundary.

In the stratified/pulsating flow region, the LE of electrostatic signals have relatively similar values, ranging between 71 and 84, indicating that the concentration of individual charged particles at the bottom of the pipeline in the stratified and pulsating flow have similar chaotic behaviour. However, a smooth transition in the LE values is present between the boundary separating stratified/pulsating flow from moving dunes to the left boundary of the blowing dunes region. This transition describes the increased chaotic behaviour of charged particles around dunes, where the dynamics of the electrostatic signal shift from the in-dividual charged particles in suspension to creeping charged particles around dunes which increase in size with the decrease in air velocity.

The LE values of the pressure signals at constant air velocities higher than the MCAV directly correlate with solids mass flow rate and the pressure drop. In addition, LE values at low solids mass flow rates ranging from 2 kg/s to 3.3 kg/s have an inverse relationship with the air velocity and the pressure drop. However, LE of pressure signals at high solids mass flow rates, ranging from 3.3 kg/s to 4.2 kg/s, have similar values across the observed flow patterns, ranging from -12 to -6.6. This similarity indicates that at high solids mass flow rates, the divergence in the pressure dynamics between individual particles and clouds of par-ticles is similar to the divergence between individual particles and dunes.

Fig. 13 shows the profile of AE and CD of phase spaces reconstructed from pressure and electrostatic signals correlated with operating con-ditions in state diagrams. The AE and CD profiles for pressure signals have an inverse relationship with their LE values, as shown in Fig. 13 (a) and (b), indicating that the highest degree of chaotic behaviour of pressure fluctuations has low AE and CD values and vice versa. In addition, AE and CD profiles of pressure signals in stratified/pulsating flow have the same trend as electrostatic signals, as shown in Fig. 13 (c)
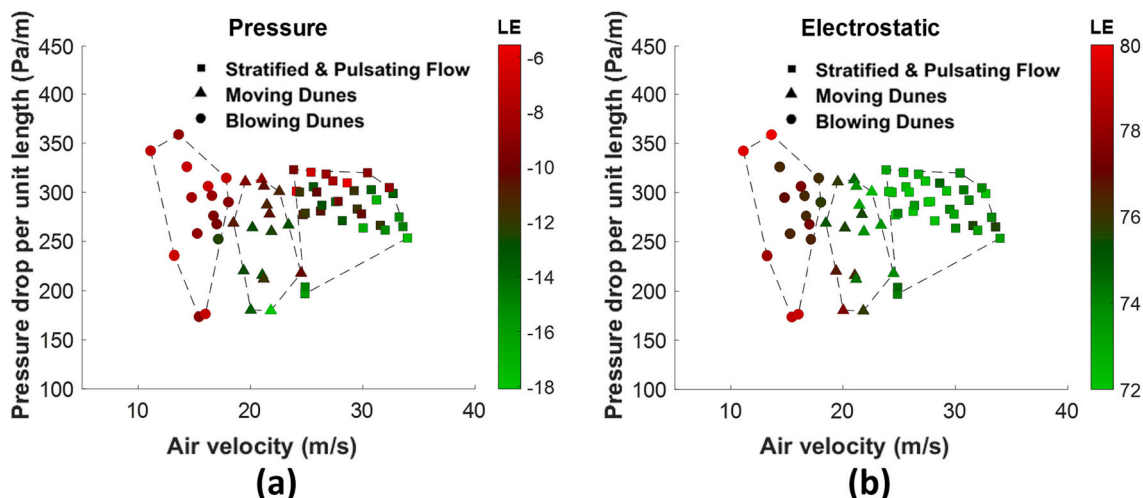

Fig. 12. State diagrams for plastic pellets correlated with large Lyapunov exponent for (a) pressure signals and (b) bottom arc-shaped electrostatic signals.
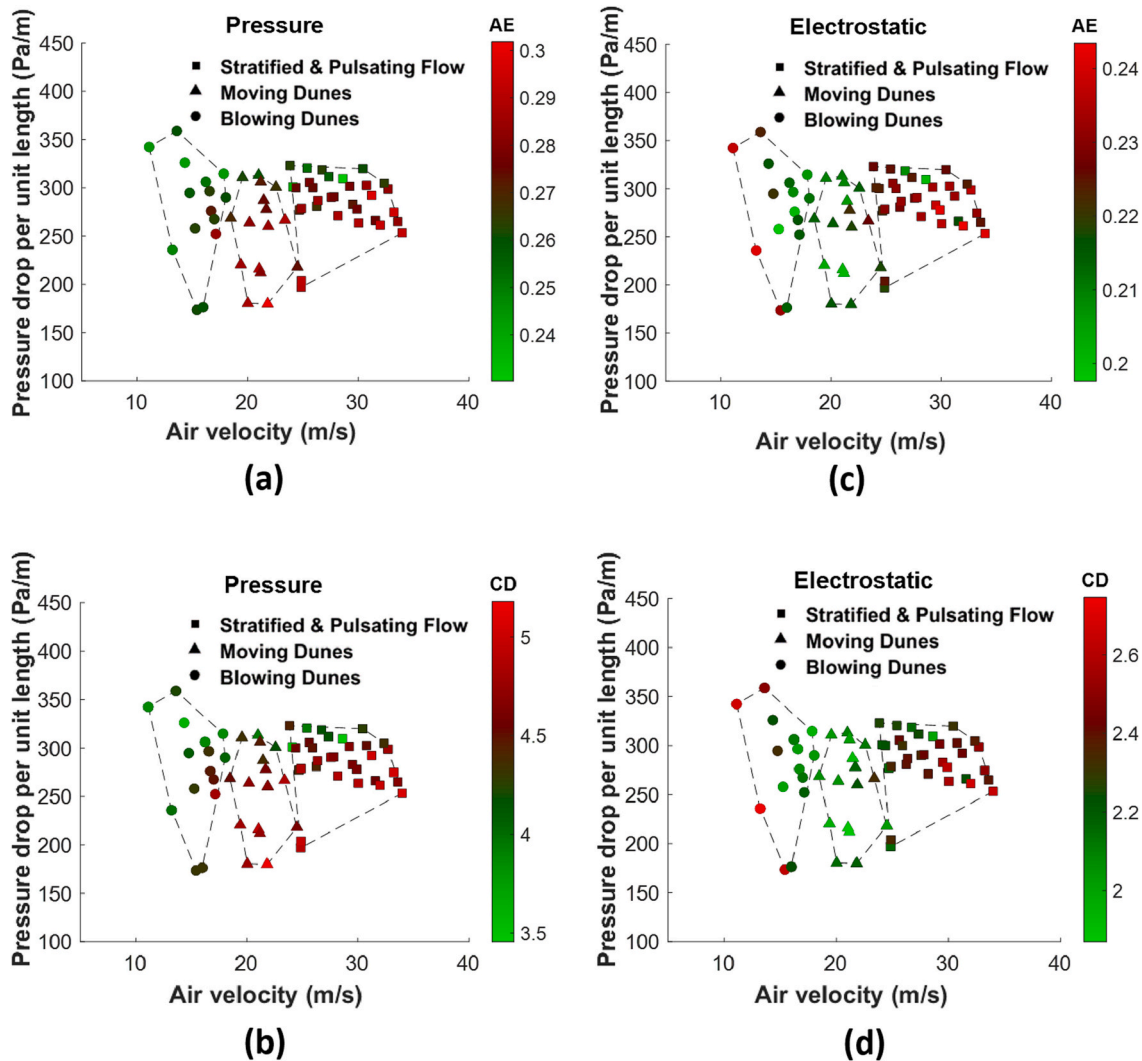
Fig. 13. State diagrams for plastic pellets correlated with approximate entropy and correlation dimension for pressure signals in (a) and (b) and for bottom arc-shaped electrostatic signals (c) and (d), respectively.

and Fig. 13 (d).

Above the MCAV in the transition between stratified/pulsating flow to moving dunes, the AE and CD values of electrostatic signals have a direct relationship with the air velocity and inverse relationship with the pressure drop. The AE and CD trend below the MCAV then shifts to a direct relationship with the pressure drop, following the same trend as their LE values, resulting in minimal values at the MCAV, ranging from 0.19 to 0.24 for AE and 1.9 to 2.75 for CD.

Fig. 14 shows the RQA measures, including RR, DET, E and L for RPs of pressure and electrostatic signals correlated with the operating conditions in state diagrams. The RR, DET, E and L values of pressure signals share the same trend and follow the same trend as their AE and CD values. Likewise, RR, DET, E and L for electrostatic signals share the same trend. However, these measures for electrostatic signals have an inverse relationship with their AE and CD values and have a much smoother transition between stratified flow, pulsating flow and moving dunes. The transition between moving dunes and blowing dunes corresponds to the highest degree of recurring dynamics, which suddenly drop at the left boundary of blowing dunes just before slugs develop at a high solids mass flow rate or form a settled layer at low solids mass flow rate.

The analysis measures obtained from the pressure signals concerning LE, CD, AE, RR, DET, E and L cannot distinguish between the observed flow patterns at high solids mass flow rates across different air velocities.

On the other hand, these measures from the electrostatic signals at different air velocities and solids mass flow rates have a much higher separation of values between the flow patterns. The effect of changing the air velocity and the solids mass flow rate on LE and DET of electrostatic signals are illustrated in Fig. 15 (a) and (b) to emphasise their ability to classify the observed flow patterns. At a decreasing air velocity and constant solids mass flow rate stratified/pulsating flow in the stratified/pulsating flow region, DET increases while LE is steady. In the transition between stratified flow and moving dunes, LE gradually increases, and DET saturates toward an approximately constant value until the transition between moving dunes and blowing dunes, indicating that the air velocity is near the MCAV. If the DET decreases with air velocity and LE still increases, it indicates that the air velocity has passed the MCAV and blowing dunes are transitioning to slug flow or settled layer.

5. Conclusions

Chaotic invariant and recurrence quantification analysis measures developed from pressure and bottom arc-shaped electrostatic signals in horizontal pneumatic conveying of plastic pellets have been successfully developed to characterise flow patterns in the transition phase between dilute and dense phase flow operations. A state diagram of plastic pellets is developed using different operating conditions and correlated with the observed flow patterns, including stratified/pulsating flow, moving
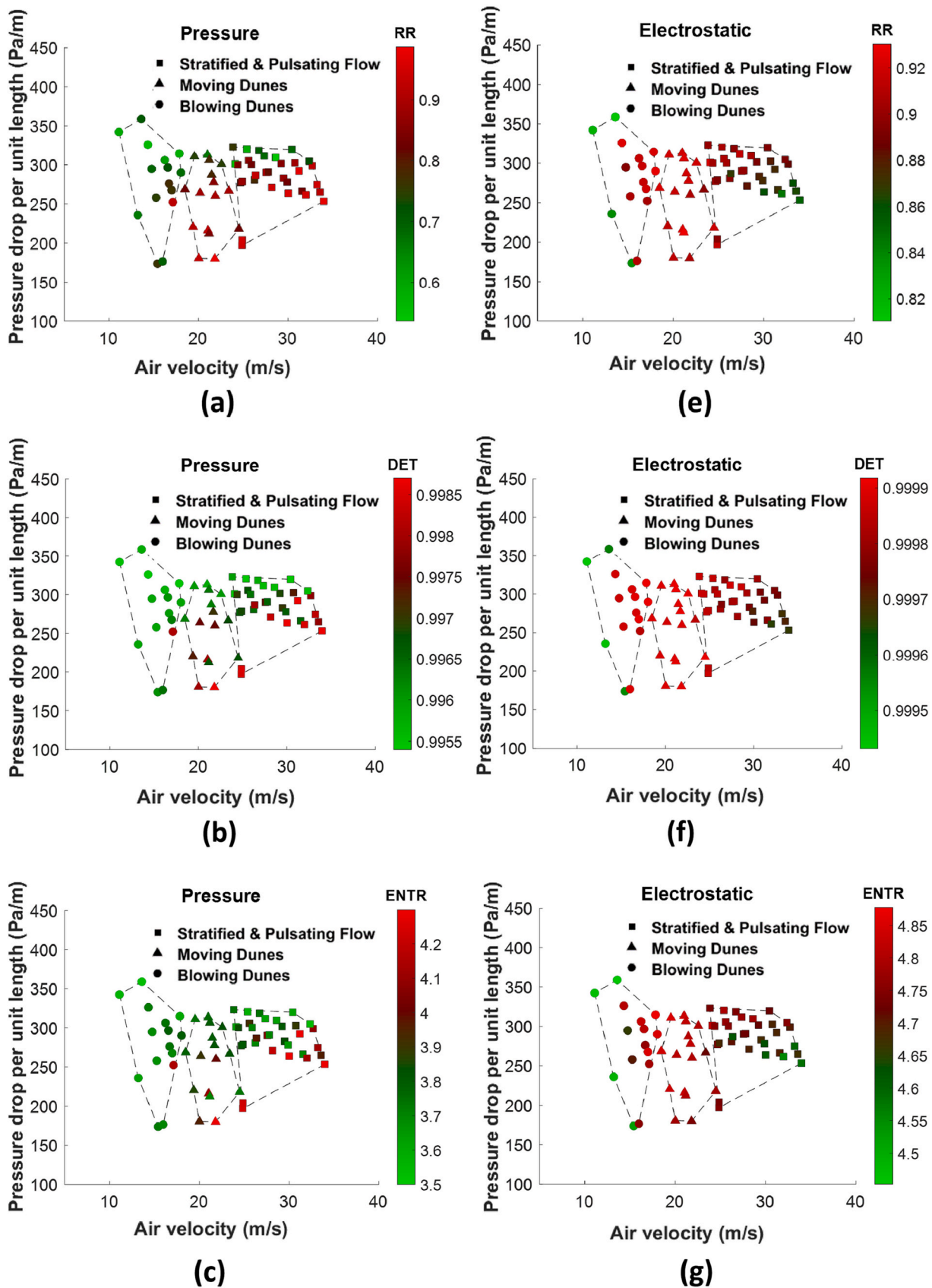
Fig. 14. State diagrams for plastic pellets correlated with recurrence quantification analysis measures including recurrence rate, determinism, entropy and average diagonal line length for pressure signals in (a), (b), (c) and (d) and for bottom arc-shaped electrostatic signals (e), (f), (g) and (h).
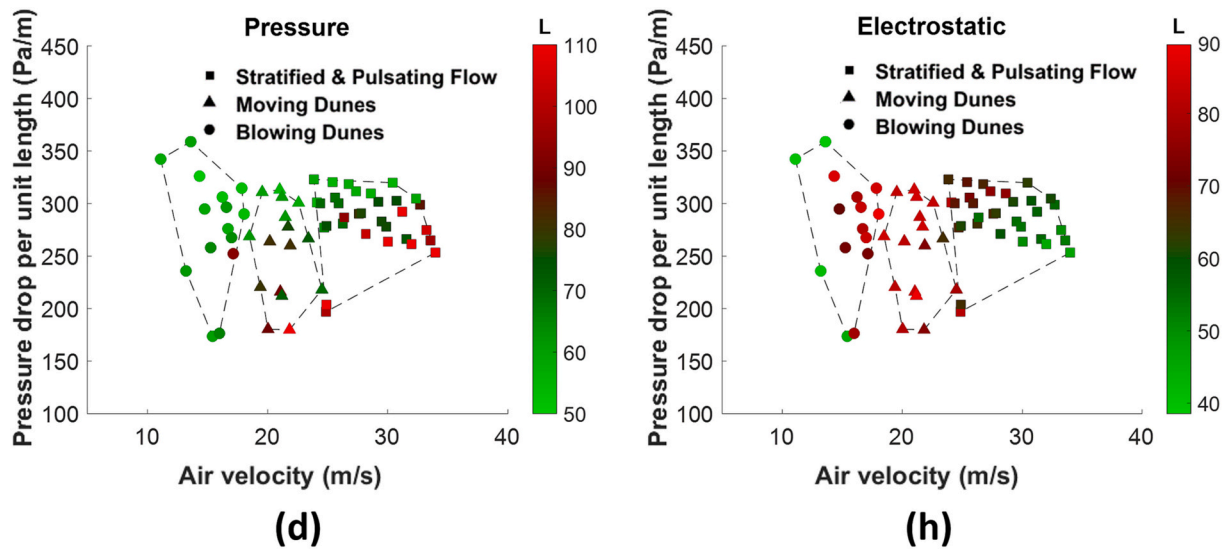
(d)

(h)

Fig. 14. (*continued*).

dunes, and blowing dunes. It is found that optimal conditions at the pressure drop minimum curve are located between moving dunes and blowing dunes.

The analysis measures are applied to phase spaces reconstructed from pressure and electrostatic signals using constant parameters, where the embedding dimension is estimated to be 10 using the false nearest neighbour algorithm. The parameters required to calculate the chaotic invariant measures concerning approximate entropy and correlation dimension and the recurrence plots are automatically estimated using the AE function across changing threshold r.

The RPs at low solids mass flow rates ranging from 2 kg/s to 3.3 kg/s and decreasing air velocity reveal various local white areas and local bolt areas, providing qualitative information on the effect of observed flow patterns on the pressure and electrostatic signals fluctuations. The local white areas reflect macroscopic disruptions in the signals, while local bolt areas are linked to mesoscopic and microscopic behaviour. The evolution of recurrence plots for pressure signals from stratified flow to moving dunes and blowing dunes transitioning to settling layers

show a decrease in the isolated local white areas values and an increase in their occurrences and structural irregularity, which means the disruptions in the pressure signals are due to the build-up of dunes. On the other hand, the local bolt areas in recurrence plots of electrostatic signals increase from stratified flow to moving dunes and decrease from moving dunes to blowing dunes transitioning to a settled layer.

The complexity of the phase spaces reconstructed from pressure and electrostatic signals is characterised using chaotic invariant measures, including the largest Lyapunov exponent, approximate entropy and correlation dimension, and their recurrence plots are quantified using recurrence quantification analysis measures, including recurrence rate, determinism, entropy and average diagonal line length. These analysis measures for pressure signals can only classify flow patterns at low solids mass flow rates ranging from 2 kg/s to 3.3 kg/s, while the measures for electrostatics can classify the flow patterns at different solids mass flow rates. Combining the largest Lyapunov exponent with recurrence quantification analysis measures for electrostatic signals is a powerful tool to indicate whether the horizontal pneumatic conveying system
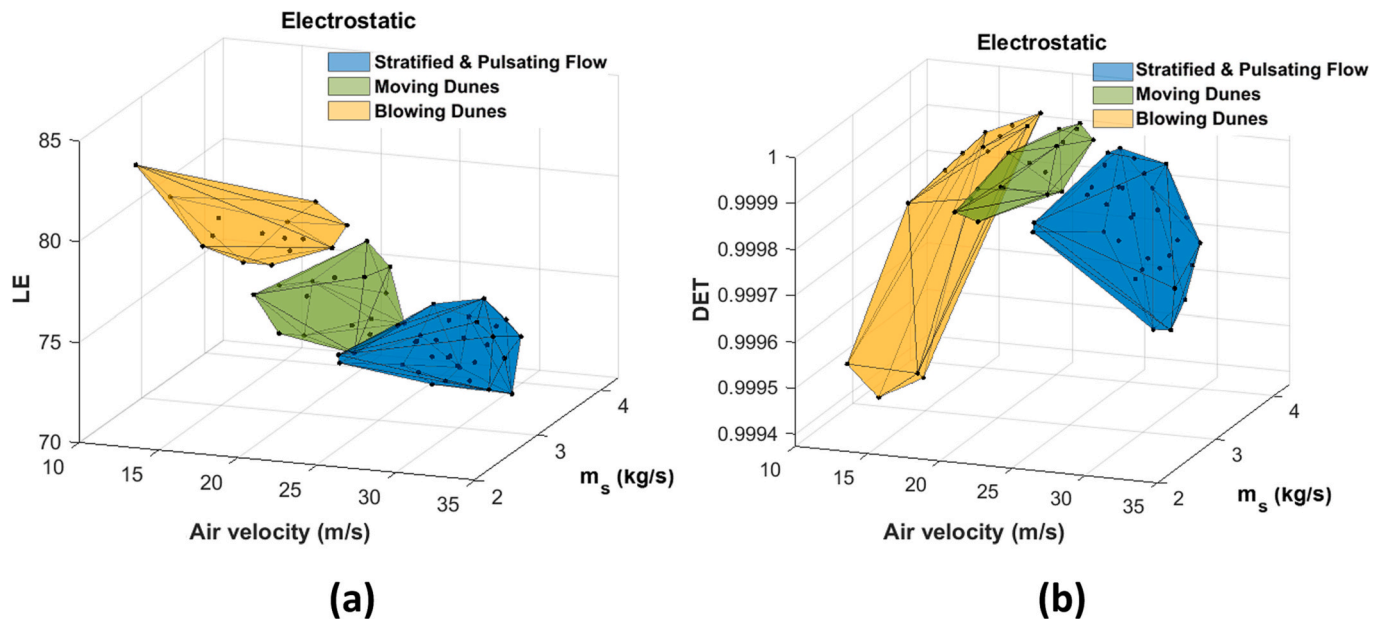

(a)

(b)

Fig. 15. A correlation of (a) largest Lyapunov exponents and (b) determinism with air velocities and m_s, classified with the observed flow patterns.

operates above, near or below the optimal operating conditions for plastic pellets.

Supplementary data to this article can be found online at https://doi.org/10.1016/j.powtec.2023.118837.

CRediT authorship contribution statement

Osamh S. Alshahed: Conceptualization, Data curation, Formal analysis, Investigation, Methodology, Project administration, Software, Validation, Visualization, Writing – original draft, Writing – review & editing. **Baldeep Kaur:** Supervision, Conceptualization, Formal analysis, Investigation, Methodology, Project administration, Validation, Visualization, Writing – review & editing. **Michael S.A. Bradley:** Supervision, Conceptualization, Formal analysis, Investigation, Methodology, Project administration, Resources, Validation, Visualization, Writing – review & editing. **David Armour-Chelu:** Formal analysis, Supervision, Validation, Visualization, Writing – review & editing.

Declaration of Competing Interest

The authors declare that they have no known competing financial interests or personal relationships that could have appeared to influence the work reported in this paper.

Data availability

Data will be made available on request.

Acknowledgements

References

[1] D. Mills, Pneumatic conveying design guide, third edit, Butterworth-Heinemann (2016), https://doi.org/10.1016/C2014-0-02678-0.

[2] A.E. Kabeel, M. Elkelawy, H.A.E.D. Bastawissi, A.M. Elbanna, An experimental and theoretical study on particles-in-air behavior characterization at different particles loading and turbulence modulation, Alex. Eng. J. 58 (2019) 451–465, https://doi.org/10.1016/j.aej.2019.04.002.

[3] G. Klinzing, F. Rizk, R. Marcus, L.S. Leung, Pneumatic Conveying of Solids: A Theoretical and Practial Approach, Third edit, Springer, 2010, https://doi.org/10.1007/978-90-481-3609-4.

[4] A. Levy, H. Kalman, Handbook of Conveying and Handling of Particulate Solids, Elsevier, First edit, 2001.

[5] P.W. Wypych, J. Yi, Minimum transport boundary for horizontal dense-phase pneumatic conveying of granular materials, Powder Technol. 129 (2003) 111–121, https://doi.org/10.1016/S0032-5910(02)00224-3.

[6] A.K. Saha, D. Das, R. Srivadtava, P.K. Panigrahi, K. Muralidhar, Fluid Mechanics and Fluid power - Contemporary Research, 2016, https://doi.org/10.1007/978-81-322-2743-4.

[7] A.B. Makwana, A. Patankar, M. Bose, Effect of dune formation on pressure drop in horizontal pneumatic conveying system, Part. Sci. Technol. 33 (2015) 59–66, https://doi.org/10.1080/02726351.2014.936541.

[8] F. Takens, Detecting strange attractors in turbulence dynamical systems and turbulence, Dyn. Syst. Turbul. 898 (1981) 366–381, https://doi.org/10.1007/bfb0091924.

[9] Bidinger Maiti, Nonlinear Time Series Analysis, Second edi, The press syndicate of the university of Cambridge, 2004.

[10] P. Grassberger, Estimation of the Kolmogorov entropy from a chaotic signal, Phys. Rev. A (Coll Park) 28 (1983) 2591–2593, https://doi.org/10.1103/PhysRevA.28.2591.

[11] S.M. Pincus, Approximate entropy as a measure of system complexity, Proc. Natl. Acad. Sci. U. S. A. 88 (1991) 2297–2301, https://doi.org/10.1073/pnas.88.6.2297.

[12] J.P. Eckmann, O. Oliffson Kamphorst, D. Ruelle, Recurrence plots of dynamical systems, Europhys. Lett. 4 (1987) 973–977, https://doi.org/10.1209/0295-5075/4/9/004.

[13] J.P. Zbilut, C.L. Webber Jr., Embeddings and delays as derived from quantification of recurrence plots, Phys. Lett. A 171 (1992) 199–203, https://doi.org/10.1016/0375-9601(92)90426-M.

[14] F.J. Cabrejos, G.E. Klinzing, Characterization of dilute gas-solids flows using the rescaled range analysis, Powder Technol. 84 (1995) 139–156, https://doi.org/10.1016/0032-5910(95)02980-G.

[15] J.B. Pahk, G.E. Klinzing, Assessing flow regimes from pressure fluctuations in pneumatic conveying of polymer pellets, Part. Sci. Technol. 26 (2008) 247–256, https://doi.org/10.1080/02726350802028926.

[16] J.S. Shijo, N. Behera, Transient parameter analysis of pneumatic conveying of fine particles for predicting the change of mode of flow, Particuology. 32 (2017) 82–88, https://doi.org/10.1016/j.partic.2016.07.004.

[17] H. Ji, H. Ohara, K. Kuramoto, A. Tsutsumi, K. Yoshida, T. Hirama, Nonlinear dynamics of gas-solid circulating fluidized-bed system, Chem. Eng. Sci. 55 (2000) 403–410, https://doi.org/10.1016/S0009-2509(99)00335-8.

[18] N. Ellis, L.A. Briens, J.R. Grace, H.T. Bi, C.J. Lim, Characterization of dynamic behaviour in gas-solid turbulent fluidized bed using chaos and wavelet analyses, Chem. Eng. J. 96 (2003) 105–116, https://doi.org/10.1016/j.cej.2003.08.017.

[19] M.F. Llop, N. Jand, K. Gallucci, F.X. Llauró, Characterizing gas-solid fluidization by nonlinear tools: chaotic invariants and dynamic moments, Chem. Eng. Sci. 71 (2012) 252–263, https://doi.org/10.1016/j.ces.2011.12.031.

[20] Y. Zhou, X. Zhu, T. Qi, Fractal characteristic analysis of multi-source information of gas-solid two-phase flow in a riser, J. Chem. Eng. Jpn. 50 (2017) 476–484, https://doi.org/10.1252/jcej.16we203.

[21] Y. Lu, P. Kang, L. Yang, X. (Eric) Hu, H. Chen, R. Zhang, Y. (Jeffrey) Zhou, X. Luo, J. Wang, Y. Yang, Multi-scale characteristics and gas-solid interaction among multiple beds in a dual circulating fluidized bed reactor system, Chem. Eng. J. 385 (2020), https://doi.org/10.1016/j.cej.2019.123715.

[22] B. Babaei, R. Zarghami, H. Sedighikamal, R. Sotudeh-Gharebagh, N. Mostoufi, Investigating the hydrodynamics of gas-solid bubbling fluidization using recurrence plot, Adv. Powder Technol. 23 (2012) 380–386, https://doi.org/10.1016/j.apt.2011.05.002.

[23] M. Tahmasebpour, R. Zarghami, R. Sotudeh-Gharebagh, N. Mostoufi, Characterization of various structures in gas-solid fluidized beds by recurrence quantification analysis, Particuology. 11 (2013) 647–656, https://doi.org/10.1016/j.partic.2012.08.005.

[24] M.F. Llop, N. Gascons, Multiresolution analysis of gas fluidization by empirical mode decomposition and recurrence quantification analysis, Int. J. Multiphase Flow 105 (2018) 170–184, https://doi.org/10.1016/j.ijmultiphaseflow.2018.04.006.

[25] F.J. Cabrejos, G.E. Klinzing, Pickup and saltation mechanisms of solid particles in horizontal pneumatic transport, Powder Technol. 79 (1994) 173–186, https://doi.org/10.1016/0032-5910(94)02815-X.

[26] C. Wang, L. Jia, W. Gao, Electrostatic sensor for determining the characteristics of particles moving from deposition to suspension in pneumatic conveying, IEEE Sensors J. 20 (2020) 1035–1042, https://doi.org/10.1109/JSEN.2019.2945572.

[27] F. Fu, M. Kong, C. Xu, C. Liang, S. Wang, Flow characterization of dense-phase pneumatic conveying system of pulverized coal through electrostatic sensor arrays, Adv. Mech. Eng. (2013) 1–12, https://doi.org/10.1155/2013/656194.

[28] S. Wang, C. Xu, J. Li, Z. Ding, S. Wang, An instrumentation system for multi-parameter measurements of gas-solid two-phase flow based on capacitance-electrostatic sensor, Measurement. 94 (2016) 812–827, https://doi.org/10.1016/J.MEASUREMENT.2016.09.010.

[29] M.A. Mergheni, J.C. Sautet, G. Godard, H. Ben Ticha, S. Ben Nasrallah, Experimental investigation of turbulence modulation in particle-laden coaxial jets by phase Doppler anemometry, Exp. Thermal Fluid Sci. 33 (2009) 517–526, https://doi.org/10.1016/J.EXPTHERMFLUSCI.2008.11.004.

[30] K. Miyazaki, G. Chen, F. Yamamoto, J.I. Ohta, Y. Murai, K. Horii, PIV measurement of particle motion in spiral gas–solid two-phase flow, Exp. Thermal Fluid Sci. 19 (1999) 194–203, https://doi.org/10.1016/S0894-1777(99)00020-5.

[31] M.S.A. Bradley, Prediction of Pressure Losses in Pneumatic Conveying Pipelines, , PhD Thesis, Thames Polytechnic, 1990, http://gala.gre.ac.uk/id/eprint/14606 (accessed June 1, 2023).

[32] A. Kumar, T. Deng, M.S.A. Bradley, Application of arc-shaped electrostatic sensors for monitoring the flow behaviour at top and bottom section of a pneumatic conveying pipeline, Measurement: Sensors 10–12 (2020) 1–8, https://doi.org/10.1016/j.measen.2020.100026.

[33] C. Rhodes, M. Morari, The false nearest neighbors algorithm: an overview, Comput. Chem. Eng. 21 (1997) 1149–1154, https://doi.org/10.1016/S0098-1354(97)87657-0.

[34] P. Grassberger, I. Procaccia, Measuring the strangeness of strange attractors, Physica D 9 (1983) 189–208, https://doi.org/10.1016/0167-2789(83)90298-1.

[35] J. Theiler, Efficient algorithm for estimating the correlation dimension from a set of discrete points, Phys. Rev. A (Coll Park) 36 (1987) 4456–4462, https://doi.org/10.1103/PhysRevA.36.4456.

[36] M.T. Rosenstein, J.J. Collins, C.J. de Luca, A practical method for calculating largest Lyapunov exponents from small data sets, Physica D 65 (1993) 117–134, https://doi.org/10.1016/0167-2789(93)90009-P.

[37] J.P. Eckmann, O. Oliffson Kamphorst, D. Ruelle, Recurrence plots of dynamical systems, Europhys. Lett. 4 (1987) 973–977, https://doi.org/10.1209/0295-5075/4/9/004.

[38] N. Marwan, M. Carmen Romano, M. Thiel, J. Kurths, Recurrence plots for the analysis of complex systems, Phys. Rep. 438 (2007) 237–329, https://doi.org/10.1016/j.physrep.2006.11.001.

[39] B. Babaei, R. Zarghami, H. Sedighikamal, R. Sotudeh-Gharebagh, N. Mostoufi, Recurrence plots to characterize gas-solid fluidization regimes, Int. J. Multiphase Flow 73 (2015) 43–56, https://doi.org/10.1016/j.ijmultiphaseflow.2015.03.003.

[40] C.L. Webber, J.P. Zbilut, Dynamical assessment of physiological systems and states using recurrence plot strategies, J. Appl. Physiol. 76 (1994) 965–973, https://doi.org/10.1152/jappl.1994.76.2.965.

[41] N. Marwan, N. Wessel, U. Meyerfeldt, A. Schirdewan, J. Kurths, Recurrence-plot-based measures of complexity and their application to heart-rate-variability data, Phys. Rev. E 66 (2002), https://doi.org/10.1103/PhysRevE.66.026702.

[42] B. Babaei, R. Zarghami, H. Sedighikamal, R. Sotudeh-Gharebagh, N. Mostoufi, Selection of minimal length of line in recurrence quantification analysis, Phys. A: Stat. Mech. Appl. 395 (2014) 112–120, https://doi.org/10.1016/j.physa.2013.10.016.

[43] M.G. Jones, K.C. Williams, Predicting the mode of flow in pneumatic conveying systems-a review, Particuology. 6 (2008) 289–300, https://doi.org/10.1016/j.partic.2008.05.003.

[44] Y. Tsuji, Y. Morikawa, S. Sugimotc, S.I. Miyoshi, Y. Nakano, Flow pattern and pressure fluctuation in air-solids two-phase flow in a pipe at low velocities, Int. J. Multiphase Flow 48 (1982) 656–663, https://doi.org/10.1299/kikaib.48.656.

[45] S. Lu, X. Chen, J.K. Kanters, I.C. Solomon, K.H. Chon, Automatic selection of the threshold value r for approximate entropy, IEEE Trans. Biomed. Eng. 55 (2008) 1966–1972, https://doi.org/10.1109/TBME.2008.919870.

[46] A. Delgado-Bonal, A. Marshak, Approximate entropy and sample entropy: a comprehensive tutorial, Entropy. 21 (2019), https://doi.org/10.3390/e21060541.

[47] B. Wu, L. Briens, J.X. Zhu, Multi-scale flow behavior in gas-solids two-phase flow systems, Chem. Eng. J. 117 (2006) 187–195, https://doi.org/10.1016/j.cej.2005.11.010.

[48] N. Marwan, How to avoid potential pitfalls in recurrence plot based data analysis, Int. J. Bifurcation Chaos 21 (2011) 1003–1017, https://doi.org/10.1142/S0218127411029008.

[49] J.P. Zbilut, J.M. Zaldivar-Comenges, F. Strozzi, Recurrence quantification based Liapunov exponents for monitoring divergence in experimental data, physics letters, section a: general, atomic and solid state, Physics. 297 (2002) 173–181, https://doi.org/10.1016/S0375-9601(02)00436-X.

[50] L. Matassini, H. Kantz, J. Hołyst, R. Hegger, Optimizing of recurrence plots for noise reduction, Phys. Rev. E 65 (2002) 1–6, https://doi.org/10.1103/PhysRevE.65.021102.

[51] Z. Gao, N. Jin, Flow-pattern identification and nonlinear dynamics of gas-liquid two-phase flow in complex networks, Phys. Rev. E 79 (2009) 1–14, https://doi.org/10.1103/PhysRevE.79.066303.

[52] R.V. Donner, Y. Zou, J.F. Donges, N. Marwan, J. Kurths, Ambiguities in recurrence-based complex network representations of time series, Phys. Rev. E Stat. Nonlinear Soft Matter Phys. 81 (2010) 2–6, https://doi.org/10.1103/PhysRevE.81.015101.